Jamming and tiling in fragmentation of rectangles

E. Ben-Naim and P. L. Krapivsky

Phys. Rev. E **100**, 032122 — Published 16 September 2019

DOI: 10.1103/PhysRevE.100.032122

Jamming and tiling in fragmentation of rectangles

E. Ben-Naim[1] and P. L. Krapivsky[2]

[1] *Theoretical Division and Center for Nonlinear Studies, Los Alamos National Laboratory, Los Alamos, New Mexico 87545, USA*

[2] *Department of Physics, Boston University, Boston, Massachusetts 02215, USA*

We investigate a stochastic process where a rectangle breaks into smaller rectangles through a series of horizontal and vertical fragmentation events. We focus on the case where both the vertical size and the horizontal size of a rectangle are discrete variables. Because of this constraint, the system reaches a jammed state where all rectangles are sticks, that is, rectangles with minimal width. Sticks are frozen as they can not break any further. The average number of sticks in the jammed state, S, grows as $S \simeq A/\sqrt{2\pi \ln A}$ with rectangle area A in the large-area limit, and remarkably, this behavior is independent of the aspect ratio. The distribution of stick length has a power-law tail, and further, its moments are characterized by a nonlinear spectrum of scaling exponents. We also study an asymmetric breakage process where vertical and horizontal fragmentation events are realized with different probabilities. In this case, there is a phase transition between a weakly asymmetric phase where the length distribution is independent of system size, and a strongly asymmetric phase where this distribution depends on system size.

I. INTRODUCTION

Fragmentation processes where large objects break into smaller ones underlie an ever growing number of physical and natural phenomena [1–7]. In particular, fragmentation occurs in soft matter systems such as polymers [8], active matter [9, 10], granular media [11, 12], and brittle materials [13–15].

Experimental and theoretical studies of fragmentation generally focus on the distribution of fragment size. Typically, this distribution is self-similar throughout the breakage process, and it is characterized by a single quantity, for example, the average fragment size [16–18]. Self-similarity extends to discrete fragments and continuous ones, one-dimensional fragments and multi-dimensional ones [19]. However, while the fragment size is a fluctuating quantity throughout the breakage process, the fragment size becomes deterministic in the final state as all fragments have the same size. In this sense, the final state can be trivial.

Recently, non-trivial final states have been reported in a multi-dimensional fragmentation process [20–23] which models martensitic phase transformations [24–26]. The system reaches a jammed state where the two-dimensional fragments are characterized two sizes: one size is a deterministic quantity, but the second size is a stochastic quantity. Here, we study this planar fragmentation process analytically, and we present a comprehensive statistical analysis of the jammed state.

We study fragmentation of rectangles with discrete horizontal and vertical sizes (Fig. 1). A rectangle can break vertically or horizontally into two smaller rectangles. Due to discreteness, rectangles with minimal vertical or horizontal size can not break, and hence, are frozen. We refer to these frozen rectangles as "sticks." Through a sequence of random fragmentation events, the system which initially consists of a single rectangle, reaches a jammed state where all rectangles are sticks (Fig. 2).

We find that, up to a logarithmic correction, the average number of frozen sticks in the jammed state, S, grows linearly with the area A,

$$S \simeq \frac{A}{\sqrt{2\pi \ln A}}\,. \tag{1}$$

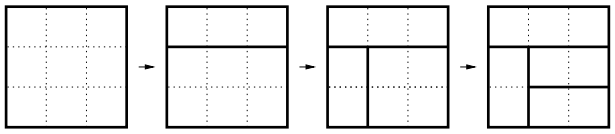

FIG. 1: Illustration of the fragmentation process (2). Initially, the system consists of a single rectangle. Through a series of horizontal and vertical cuts, the system reaches a jammed state where fragmentation is no longer possible.

Interestingly, this asymptotic behavior is universal as it applies regardless of aspect ratio. We also study the distribution of stick length and find that this distribution has a power-law tail. Further, this length distribution exhibits multi-scaling asymptotic behavior as its moments are characterized by a nonlinear spectrum of exponents.

We also investigate an asymmetric process where horizontal and vertical cuts are realized with different probabilities. We find a phase transition at a critical value of the asymmetry parameter. In the weakly asymmetric phase, the length distribution does not depend on system size, while in the strongly asymmetric phase, this distribution does depend on system size.

The rest of this paper is organized as follows. In Sec. II, we introduce the fragmentation process and develop the theoretical techniques used throughout this investigation to obtain the leading asymptotic behavior in the large system-size limit. We first analyze the average number of sticks and then consider the length distribution of sticks. In Sec. III, we generalize the results to the case where horizontal and vertical fragmentation occur at different rates. Next, in section IV, we analyze a closely related process of fragmentation into four, rather than two, rect-

angles. In this case, the outcome of a fragmentation event is deterministic, and we can also address the total number of jammed configurations. We conclude with a discussion in Sec. V. Details of several technical derivations are presented in the Appendix.

II. FRAGMENTATION OF RECTANGLES

Initially, the system consists of a single rectangle with horizontal size m, vertical size n, and hence, area $A = mn$. Both the horizontal size and the vertical size are integer. It is convenient to envision a square grid with $(m-1)(n-1)$ internal grid points embedded within the rectangle (Fig. 1). In each fragmentation event, an internal grid point is selected, and then a cut is made along the horizontal or the vertical direction. As a result, the rectangle breaks into two smaller ones,

$$(m,n) \to \begin{cases} (i,n)+(m-i,n) & \text{with prob. } 1/2, \\ (m,j)+(m,n-j) & \text{with prob. } 1/2. \end{cases} \quad (2)$$

The grid point with $1 \le i \le m-1$ and $1 \le j \le n-1$ is chosen at random, as is the fragmentation direction. Of course, the total area is conserved.

Fragmentation requires an internal grid point. Therefore, rectangles with $m > 1$ and $n > 1$ are active, and otherwise, rectangles with $m = 1$ or $n = 1$, referred to as sticks, are frozen. The fragmentation process (2) is repeated for every active rectangle until the system reaches a jammed state with sticks only (Fig. 2). In this study, we focus on the jammed state.

Let $S(m,n)$ be the average number of sticks in the jammed state when the initial rectangle has dimensions $m \times n$. This average is taken over all realizations of the random breakage process. Since the fragmentation process (2) is symmetric with respect to the horizontal and the vertical direction, we expect $S(m,n) = S(n,m)$. The average number of frozen sticks obeys the recursion [26]

$$S(m,n) = \frac{1}{m-1}\sum_{i=1}^{m-1} S(i,n) + \frac{1}{n-1}\sum_{j=1}^{n-1} S(m,j)\,. \quad (3)$$

The first term on the right-hand side accounts for the $m-1$ possible cuts in the vertical direction, and similarly, the second term accounts for the $n-1$ possible cuts in the horizontal direction. The recursion equation is subject to the boundary conditions

$$S(m,1) = S(1,n) = 1 \quad (4)$$

for all $m \ge 1$ and $n \ge 1$. Each fragmentation event involves a single rectangle, and accordingly, the governing equation is linear. We emphasize that the governing equation (3) is exact: since there are no two-body interactions, our theoretical treatment makes no mean-field assumptions regarding two-body correlations.

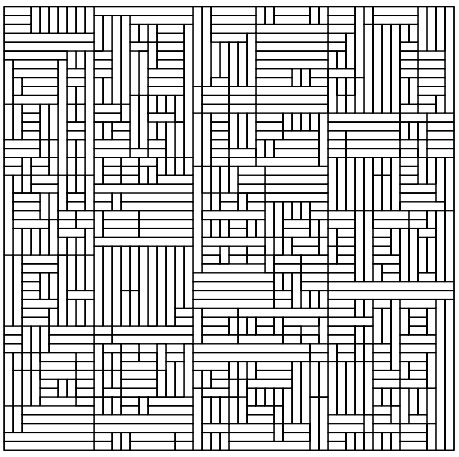

FIG. 2: A jammed state in a system of size 50×50. The jammed state consists of rectangles of size $1 \times k$ or $k \times 1$.

Equations (3) and (4) yield the average number of frozen sticks for small rectangles,

$$\begin{aligned} &S(2,2) = 2, \quad S(2,3) = \tfrac{5}{2}, \quad S(2,4) = \tfrac{17}{6}, \\ &S(3,3) = \tfrac{7}{2}, \quad S(3,4) = \tfrac{17}{4} \quad S(4,4) = \tfrac{97}{18}\,. \end{aligned} \quad (5)$$

Moreover, for ladders ($m = 2$), equation (3) simplifies to $S(2,n) - S(2,n-1) = \frac{1}{n-1}$ and therefore,

$$S(2,n) = 1 + H_{n-1}\,, \quad (6)$$

where $H_N = \sum_{1\le i\le N} i^{-1}$ is the harmonic number. For long ladders, $S(2,n) \simeq \ln n + 1 + \gamma$, where $\gamma = 0.57721$ is the Euler constant. It is also possible to show that as long as m is finite, the leading asymptotic behavior remains logarithmic,

$$S(m,n) \simeq \frac{(\ln n)^{m-1}}{(m-1)!^2}\,, \quad (7)$$

in the limit $n \to \infty$.

Our main interest is the behavior for large rectangles, and specifically, the leading asymptotics when $m \to \infty$ and $n \to \infty$. Hence, we treat m and n as continuous variables, and replace the sums in (3) with integrals. The average number of sticks satisfies the integral equation

$$S(m,n) = \frac{1}{m}\int_1^m di\, S(i,n) + \frac{1}{n}\int_1^n dj\, S(m,j)\,, \quad (8)$$

within this continuous framework. Next, we multiply this integral equation by the area mn and then differentiate the resulting equation with respect to m and n. That shows the quantity $S(m,n)$ satisfies the partial differential equation

$$\partial_m\partial_n\,[mnS(m,n)] = \partial_m\,[mS(m,n)] + \partial_n\,[nS(m,n)]\,. \quad (9)$$

We emphasize that the continuum approach yields the leading asymptotic behavior for large n and m exactly,

but it is not expected to give the leading correction. To illustrate this, we take for example the recursion above (6), which in the continuum approach translates to the differential equation $dS(2,n)/dn = 1/n$. Indeed, this equation yields the leading asymptotic behavior exactly, $S(2,n) \simeq \ln n$, but it does not produce the correction which involves the Euler constant.

Hereinafter, we use $\partial_m = \frac{\partial}{\partial m}$ and $\partial_n = \frac{\partial}{\partial n}$ to denote partial derivatives. Further simplification can be achieved by introducing the logarithmic variables

$$\mu = \ln m, \qquad \nu = \ln n\,. \tag{10}$$

With this transformation, Eq. (9) reduces to a partial differential equation with constant coefficients,

$$\partial_\mu \partial_\nu S(\mu,\nu) = S(\mu,\nu)\,, \tag{11}$$

that should be solved subject to the boundary conditions $S(\mu,0) = 1$ and $S(0,\nu) = 1$.

The central quantity throughout our analysis is the double Laplace transform

$$\widehat{S}(p,q) = \int_0^\infty d\mu\, e^{-p\mu} \int_0^\infty d\nu\, e^{-q\nu}\, S(\mu,\nu)\,. \tag{12}$$

It is obtained by multiplying both sides of the governing equation (11) by $e^{-p\mu-q\nu}$ and then integrating over the logarithmic variables μ and ν. By using the boundary conditions $S(\mu,0) = 1$ and $S(\nu,0) = 1$, we find that double Laplace transform is remarkably compact,

$$\widehat{S}(p,q) = \frac{1}{pq-1}. \tag{13}$$

Therefore, the average number of sticks in the jammed state, $S(\mu,\nu)$, equals the inverse Laplace transform

$$\begin{aligned} S(\mu,\nu) &= \int_{-\mathrm{i}\infty}^{\mathrm{i}\infty} \frac{dp}{2\pi\mathrm{i}} \int_{-\mathrm{i}\infty}^{\mathrm{i}\infty} \frac{dq}{2\pi\mathrm{i}}\, \frac{e^{p\mu+q\nu}}{pq-1} \\ &= \int_{-\mathrm{i}\infty}^{\mathrm{i}\infty} \frac{dq}{2\pi\mathrm{i}}\, \frac{1}{q}\, e^{\nu q+\mu/q}\,. \end{aligned} \tag{14}$$

We perform the inversion first with respect to the conjugate variable p and then with respect to the conjugate variable q. The inversion with respect to p is immediate as the integrand in the first line has a pole at $p = q^{-1}$.

The integral over the variable q in (14) has the form

$$I = \int_{-\mathrm{i}\infty}^{\mathrm{i}\infty} \frac{dq}{2\pi\mathrm{i}}\; F(q)\, e^{\nu f(q)}\,. \tag{15}$$

The exponential dominates the integrand in the limit $\nu \to \infty$. Further, the function $f(q)$ is maximal at the saddle point q_* which is determined from $f'(q_*) = 0$, and in the vicinity of this saddle point we have

$$f(q) \simeq f(q_*) + \tfrac{1}{2}(q-q_*)^2 f''(q_*)\,. \tag{16}$$

The integration contour in (15) can be along any line that parallels the imaginary axis in the complex plane as long as $\mathrm{Re}(q)$ is greater than the real part of any singularity the integrand may have. We conveniently choose a line parallel to the imaginary axis that passes through the saddle point q_*. With the transformation of variables $q = q_* + \mathrm{i}y/\sqrt{f''(q_*)}$, the integral (15) reduces to a Gaussian integral. As long as $\mathrm{Re}(q_*)$ exceeds the real part of the singularities of $F(q)$, we have

$$I \simeq \frac{F(q_*)\, e^{\nu f(q_*)}}{\sqrt{2\pi\nu f''(q_*)}}\,. \tag{17}$$

Here, we used $\int_{-\infty}^{\infty} \exp(-y^2/2)dy = \sqrt{2\pi}$.

First, we discuss squares, $\mu = \nu$, for which $S(\nu,\nu) = I$ with I given in (15). The quantities $F(q) = q^{-1}$ and

$$f(q) = q + q^{-1} \tag{18}$$

specify the integral (15). The saddle point is $q_* = 1$, and furthermore, $f(q_*) = f''(q_*) = 2$ and $F(q_*) = 1$. By substituting these values into the general expression (17), we obtain the leading asymptotic behavior

$$S(\nu,\nu) \simeq \frac{e^{2\nu}}{\sqrt{4\pi\nu}}\,. \tag{19}$$

Equation (1) expresses this behavior in terms of the area $A = e^{2\nu}$. Results of numerical evaluation of the recursion equation (3) are in excellent agreement with the theoretical prediction, and we conclude that the continuum framework yields exact results for the leading asymptotic behavior (Fig. 3).

We now consider rectangles of arbitrary size for which $S(\mu,\nu) = I$ with $f(q) = q + (\mu/\nu)q^{-1}$ and $F(q) = q^{-1}$. It is straightforward to repeat the steps leading to (19), and obtain the general behavior

$$S(\mu,\nu) \simeq \frac{e^{2\sqrt{\mu\nu}}}{\sqrt{4\pi\sqrt{\mu\nu}}}\,. \tag{20}$$

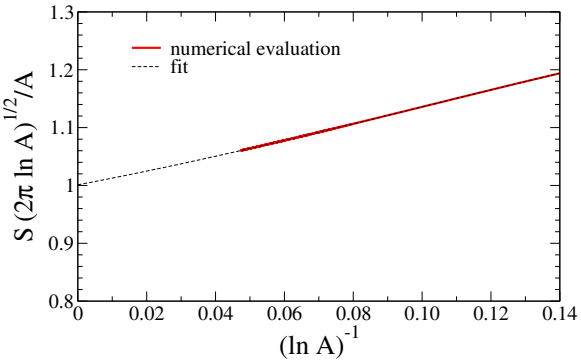

FIG. 3: The quantity $S\sqrt{2\pi \ln A}\,/A$ versus $(\ln A)^{-1}$. The dashed line shows results of a fourth-order polynomial fit to the data, and the intercept agrees with the theoretical prediction of unity to within 0.1%. The quantity S was obtained by numerical iteration of the recursion equation (3), subject to the boundary condition (4).

As expected, the average number of sticks is symmetric, $S(\mu,\nu) = S(\nu,\mu)$, and moreover, the quantity ν in (19) is now replaced with the geometric average $\sqrt{\mu\nu}$. In the limit $m \to \infty$ and $n \to \infty$ with the aspect ratio $r = \frac{m}{n}$ kept fixed, we have $\sqrt{\mu\nu} \simeq (\mu+\nu)/2$. In this limit, the leading asymptotic behavior (20) is identical to (19). Interestingly, the average number of jammed sticks is universal in the large-area limit—all rectangles with the same area behave similarly. The only requirement is that the aspect ratio is finite. In view of this universality, we henceforth quote results for squares without loss of generality.

In the jammed state, the original rectangle is covered with rectangles of size $1 \times k$ or $k \times 1$ with $k \geq 2$, and we now analyze the distribution of stick length k. Let $S_k(m,n)$ be the average number sticks of length k when the initial rectangle has dimensions $m \times n$. Similar to $S(m,n)$, the quantity $S_k(m,n)$ is an average over all realizations of the random breakage process (2) resulting in the jammed state. For example, for a rectangle of size 3×2, according to Eq. (2), with probability $\frac{1}{2}$, the jammed state has two sticks of length three and with an equal probability, the jammed state has three sticks of length two. Hence, $S_2(3,2) = \frac{3}{2}$ and $S_3(3,2) = 1$.

The quantity $S_k(m,n)$ satisfies two sum rules,

$$S(m,n) = \sum_{k\geq 2} S_k(m,n)\,, \quad A = \sum_{k\geq 2} k S_k(m,n)\,. \tag{21}$$

Let $\langle k\rangle = \sum_k k S_k / \sum_k S_k$ be the first moment of the normalized quantity $S_k(m,n)/S$. Equation (21) implies that $\langle k\rangle = A/S$, and hence, this quantity grows logarithmically with area, $\langle k\rangle \simeq \sqrt{2\pi \ln A}$. Such behavior is independent of the aspect ratio in the large-area limit.

For all k, the quantity $S_k(m,n)$ satisfies the recursion equation (3), although the boundary condition does depend on length

$$S_k(m,1) = \delta_{m,k} \qquad S_k(1,n) = \delta_{n,k}\,. \tag{22}$$

With the boundary condition $S_n(1,n) = 1$, the recursion equation (3) implies $S_n(m,n) = 1$ for all $m < n$, and it is also possible to show that $S_n(n,n) = 2$.

The linear equation (3) which governs $S(m,n)$ and $S_k(m,n)$ is manifestly exact. It is still useful to compare its predictions with results of numerical Monte Carlo simulations of the breakage process. In the simulations, we start with a rectangle of size $m \times n$ and perform the fragmentation step (2) repeatedly until all rectangles are sticks. We then tally the number of sticks of a given length, and the quantity $S_k(m,n)$ equals this tally, divided by the number of independent realizations of the random process. For example, for a square of size 5×5 we were able to validate the theoretical predictions $S_2(5,5) = \frac{95}{32}$, $S_3(5,5) = \frac{235}{144}$, $S_4(5,5) = \frac{25}{24}$, and $S_5(5,5) = 2$ to within 10^{-5} using 10^{11} independent realizations. Indeed, the linear recursion equation (3) yields the average number of sticks of length k exactly. Since the quantity $S_k(m,n)$ measures the abundance of sticks of length k, we define $S_k(m,n)/S(m,n)$ as the distribution of stick length throughout this paper. We caution that this distribution corresponds to the aforementioned measurement procedure in numerical simulations.

For large rectangles, we utilize the continuum approach once again. As a function of the logarithmic variables defined in (10), the average number of frozen sticks with a given length $S_k(\mu,\nu)$ satisfies the partial differential equation (11), subject to the boundary conditions

$$\begin{aligned} S_k(\mu,0) &= e^{-\mu}\delta(\mu - \ln k), \\ S_k(0,\nu) &= e^{-\nu}\delta(\nu - \ln k)\,. \end{aligned} \tag{23}$$

To obtain these boundary conditions, we first rewrite (22) as $S_k(m,1) = \delta(m-k)$ and $S_k(1,n) = \delta(n-k)$ and then perform the transformation of variables (10) by using $\delta[\mathcal{F}(x)] = \delta(x-x_0)/|\mathcal{F}'(x_0)|$.

Next, we repeat the steps leading to (13), using the partial differential equation (11) which also governs $S_k(\mu,\nu)$ and the boundary condition (23), and arrive at

$$\widehat{S}_k(p,q) = \frac{pk^{-1-p} + qk^{-1-q}}{pq-1}\,. \tag{24}$$

We note that this double Laplace transform is symmetric, $\widehat{S}_k(p,q) = \widehat{S}_k(q,p)$, as the two terms in the numerator are equivalent. Since the continuum approximation is exact only asymptotically, that is, in the limit $k \to \infty$, the resulting Laplace transform does not necessarily satisfy the normalization $\sum_k \widehat{S}_k(p,q) = \widehat{S}(p,q)$ (see also Appendix A). For squares, $\mu = \nu$, it suffices to invert only one of these terms. We thus perform the inverse Laplace transform of the term $qk^{-1-q}/(pq-1)$ first with respect to p and then with respect to q, thereby leading to $S_k(\nu,\nu) = I$ with I given by (17). The integrand is specified by $F(q) = 2$ and

$$f(q) = q + q^{-1} - (1+q)x\,, \quad x = \frac{\ln k}{\ln n}\,. \tag{25}$$

The saddle point is $q_* = 1/\sqrt{1-x}$, and by substituting $f(q_*) = 2\sqrt{1-x} - x$ and $f''(q_*) = 2(1-x)^{3/2}$ into the general formula (17), we obtain

$$S_k(\nu,\nu) \simeq \frac{\exp\left[\nu\left(2\sqrt{1-x}-x\right)\right]}{\sqrt{\pi\nu(1-x)^{3/2}}}\,. \tag{26}$$

The distribution of frozen sticks with length k is defined by $P_k(\nu) = S_k(\nu,\nu)/\sum_k S_k(\nu,\nu)$, and we reiterate that the quantities S_k are obtained as averages over all realizations of the random breakage process (2). This quantity is normalized, $\sum_{k\geq 2} P_k = 1$, and its first moment is $\langle k\rangle = \sum_{k\geq 2} k P_k$. By using equations (19) and (26) we find that the length distribution adheres to the scaling form

$$\frac{\ln\left(\frac{1}{2}P_k\right)}{\ln n} \simeq \Phi\left(\frac{\ln k}{\ln n}\right) \tag{27}$$

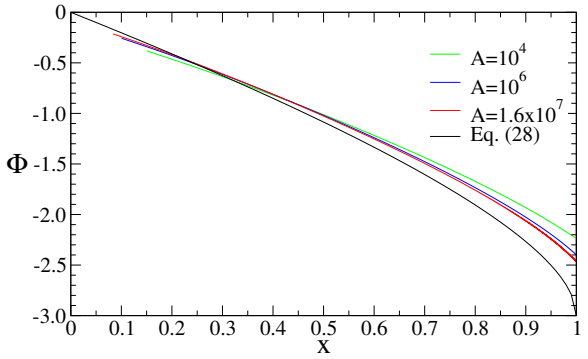

FIG. 4: The scaling function $\Phi(x)$ versus the scaling variable x. Results from three different system sizes are compared with the theoretical prediction. To evaluate $\Phi(x)$, the quantity $S_k(m,n)$ was obtained by numerical iteration of the recursion equation (3), subject to the boundary condition (22).

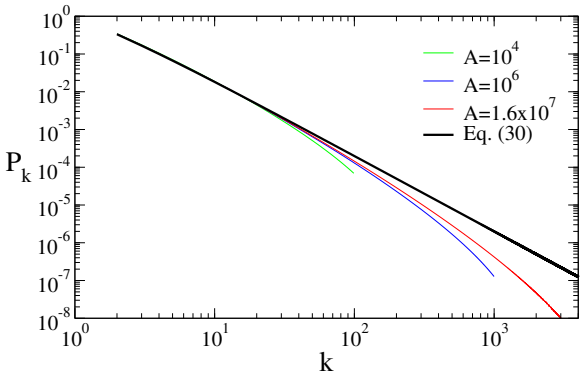

FIG. 5: The length distribution P_k versus k. Numerical results for three system sizes are compared with the theoretical prediction. To evaluate P_k, the quantity $S_k(m,n)$ was obtained by numerical iteration of the recursion equation (3), subject to the boundary condition (22). Not displayed is the anomalous data point $P_n = 2/S(n,n)$ corresponding to the largest possible stick which shows a sharp jump as $P_n \simeq 2\sqrt{2\pi \ln A}\, A^{-1}$ (see also [26]).

with the scaling function

$$\Phi(x) = 2\left(\sqrt{1-x} - 1\right) - x\,. \tag{28}$$

Equation (27) constitutes an unusual scaling form as the scaled logarithm of the length distribution P_k is a universal function of the scaled logarithm of the length k. As a result, the convergence toward the ultimate asymptotic behavior is extremely slow as it involves logarithm of system size (Fig. 4).

The scaling behavior (27)-(28) describes the distribution at large length scales, that is, $\ln k = \mathcal{O}(\ln n)$. Still, the small-$x$ behavior $\Phi(x) \simeq -2x - \frac{1}{4}x^2$ yields the behavior at smaller length scales,

$$P_k \simeq 2k^{-2} \exp\left[-\frac{(\ln k)^2}{4\ln n}\right]. \tag{29}$$

Therefore, the length distribution decays as a power-law, $P_k \simeq 2k^{-2}$ [26], at sufficiently small length scales, $\ln k \ll \sqrt{\ln n}$. Beyond this length scale, the power-law tail is suppressed by a log-normal term. We also note that log-normal distributions naturally arise in multiplicative random processes [27, 28], and that the fragmentation process (2) can be formulated as such, for example, $(m,n) \to (mx,n) + \big(m(1-x),n\big)$ with $x = i/m$, in the first line of (2).

In a finite system, the power-law tail holds over a limited range (Fig. 5). Further, the log-normal term is relevant at length scales k_2 determined by $\ln k_2 \sim \sqrt{\ln n}$. Similarly there is a series of length scales k_b that are specified by $\ln k_b \sim (\ln n)^{(b-1)/b}$. For $k \sim k_b$, the $b^{\rm th}$ term in the Taylor expansion of $\Phi(x)$ affects the length distribution. For instance, when $k \sim k_4$ we have

$$P_k \simeq 2\exp\left[-2\ln k - \frac{(\ln k)^2}{4\ln n} - \frac{(\ln k)^3}{8(\ln n)^2} - \frac{5(\ln k)^4}{64(\ln n)^3}\right].$$

Ultimately, at sufficiently large scales, the entire scaling function (28) characterizes the length distribution (Fig. 4).

In appendix A, we derive the exact length distribution

$$P_k = \frac{2}{k(k+1)}\,, \tag{30}$$

which is realized in the limit $n \to \infty$. This distribution is properly normalized, $\sum_{k\geq 2} P_k = 1$, and its power-law tail $P_k \simeq 2k^{-2}$ agrees with the asymptotic behavior (29). We stress that (30) is exact for all $k \geq 2$ whereas (29) is only asymptotically exact, yielding the leading behavior in the limit $k \to \infty$. Furthermore, results of numerical evaluation of the recursion equation (3) with the boundary condition (22) are in excellent agreement with this theoretical prediction (Fig. 5). Moreover, we numerically validated the theoretical prediction $P_2 = \frac{1}{3}$ to within 0.1% using the extrapolation described in the caption to figure 3. The exact length distribution (30) can be expressed as a ratio of Gamma functions, the discrete counterpart of a power-law. It can be derived by treating the variables m and n as discrete, in contrast with the continuum analysis leading to (29).

Finally, we investigate the moments of the quantity P_k, defined by $\langle k^h\rangle = \sum_{k\geq 2} k^h P_k$. It is convenient to normalize these moments by $\langle k\rangle$,

$$M_h = \frac{\langle k^h\rangle}{\langle k\rangle}\,, \tag{31}$$

with $h > 1$. By using the definition $P_k = S_k/S$ and the second sum rule in (21), we can express the normalized moments through $S_k(n,n)$,

$$M_h = n^{-2}\sum_{k\geq 2} k^h S_k(n,n)\,. \tag{32}$$

We now substitute (26) into this expression and convert the sum over the discrete variable k into an integral over

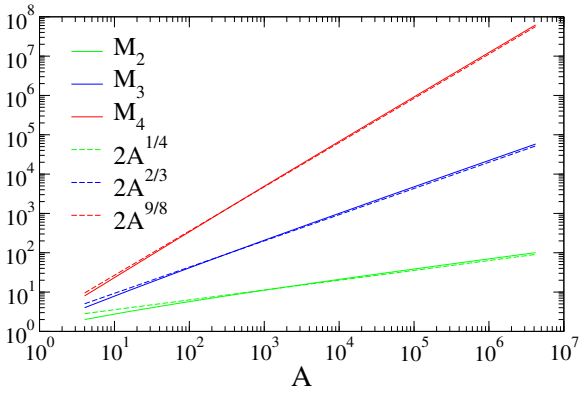

FIG. 6: The normalized moments M_h versus square area A for $h = 2, 3, 4$. Also shown as a reference are the corresponding theoretical predictions.

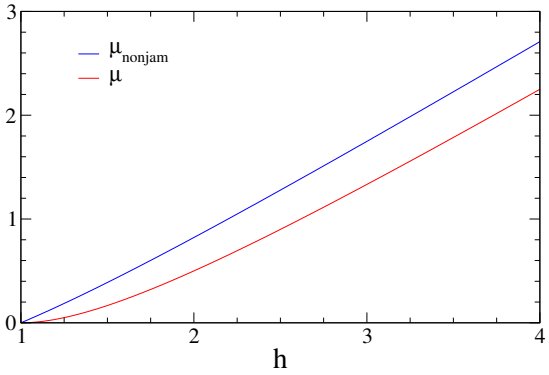

FIG. 7: The scaling exponents μ and $\mu_{\rm nonjam}$ versus the moment index h.

the continuous variable x by using $k = e^{\nu x}$. With this transformation of variables, the moments are given by

$$M_h \simeq \sqrt{\frac{\nu}{\pi}} \int_0^1 dx\, (1-x)^{-3/4}\, e^{\nu\phi(x)}\,, \qquad (33)$$

with $\phi(x) = \Phi(x) + (h+1)x$. The exponential term dominates the integral in the limit $\nu \to \infty$. The function $\phi(x)$ is maximal at the saddle point, $x_* = 1 - h^{-2}$, and from the quadratic behavior $\phi(x) = \phi(x_*) + \frac{1}{2}\phi''(x_*)(x - x_*)^2$, we deduce the leading asymptotic behavior (Fig. 6)

$$M_h \simeq 2\, A^{\mu(h)} \quad \text{with} \quad \mu(h) = \frac{(h-1)^2}{2h}\,. \qquad (34)$$

Results of numerical evaluation of low-order moments are in excellent agreement with this theoretical prediction.

The scaling exponent μ is a nonlinear function of the index h, and therefore, the scaling behavior of the first moment does not characterize high-order moments. Hence, the moments exhibit multi-scaling asymptotic behavior.

It is interesting to compare the behavior with that found for a counterpart of the fragmentation process (2) where any point inside a rectangle may be selected at random, and consequently, the horizontal and vertical sizes of rectangles are not restricted to integers. In this case, the number of fragments grows linearly with the number of fragmentation events t, and conversely, the average area of a fragment, $\langle a\rangle$, is inversely proportional to this quantity, $\langle a\rangle \sim t^{-1}$. In contrast with the behavior discussed above, the fragmentation process never stops and the system does not reach a jammed state [25, 30].

To compare the two cases, we note that the aspect ratio of a frozen rectangle r equals its length, $r = k$. For the nonjamming process, the normalized moments of the aspect ratio, $M_h = \langle r^h\rangle/\langle r\rangle$, also exhibit multi-scaling asymptotic behavior $M_h \sim (A/\langle a\rangle)^{\mu_{\rm nonjam}}$, where $\langle a\rangle$ is the average area of a rectangle and

$$\mu_{\rm nonjam} = \sqrt{h^2+1} - \sqrt{2} \qquad (35)$$

is the nonlinear scaling exponent [25, 30]. Notably, the two spectra of exponents are different, $\mu \neq \mu_{\rm nonjam}$ although both become linear at high orders, $\mu \simeq \mu_{\rm nonjam} \simeq h$ as $h \to \infty$. Figure 7 shows that multi-scaling is more pronounced in the present case.

III. ASYMMETRIC FRAGMENTATION

We now generalize the fragmentation process (2) and consider the case where the probabilities of horizontal and vertical cuts may differ [26]. The asymmetric fragmentation process can be represented schematically as

$$(m,n) \to \begin{cases} (i,n) + (m-i,n) & \text{prob. } (1-\alpha)/2, \\ (m,j) + (m,n-j) & \text{prob. } (1+\alpha)/2. \end{cases} \qquad (36)$$

The parameter α controls the degree of asymmetry, and without loss of generality, we assume $0 \le \alpha \le 1$. The fragmentation process (36) reduces to (2) when there is no asymmetry, $\alpha = 0$, and it becomes one-dimensional, when the asymmetry parameter is maximal, $\alpha = 1$.

In the completely asymmetric case, the jammed state contains n identical sticks of length n. Hence, the number of sticks is not proportional to the area, and also, there is no logarithmic dependence on system size, unlike (1). Below, we show that the logarithmic dependence on system size disappears when the asymmetry parameter exceeds the critical value

$$\alpha_c = \frac{1}{\sqrt{2}}\,. \qquad (37)$$

The average number of frozen sticks obeys

$$S(m,n) = \frac{1-\alpha}{m-1}\sum_{i=1}^{m-1} S(i,n) + \frac{1+\alpha}{n-1}\sum_{j=1}^{n-1} S(m,j), \quad (38)$$

subject to the boundary condition (4). This recurrence reduces to (3) when the asymmetry parameter vanishes.

Once again, we employ the continuum approach. In terms of the logarithmic variables (10), the quantity

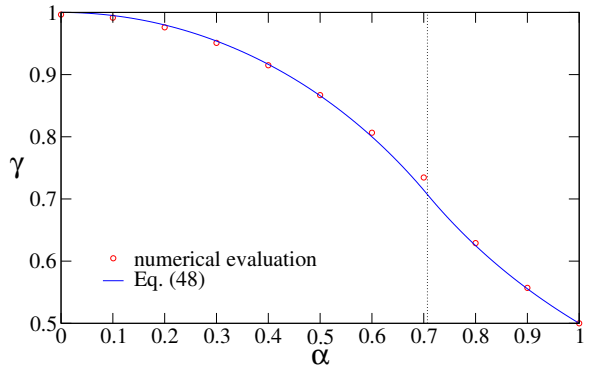

FIG. 8: The exponent γ given by (48) versus the asymmetry parameter α. Also shown are results of numerical evaluation of the recursion equations with $A = 10^8$. To estimate the power-law exponent, we took into account the logarithmic correction in the weakly asymmetric phase, according to (49). The critical point (37) is indicated by the dashed vertical line.

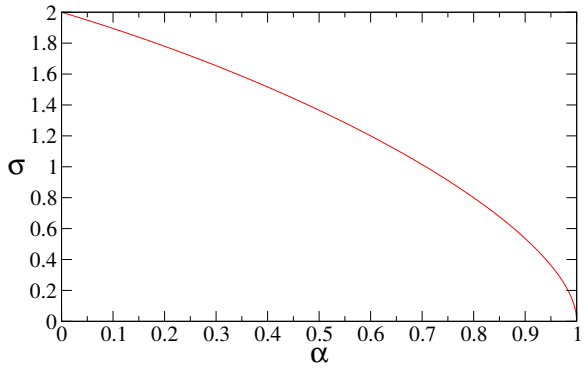

FIG. 9: The power-law exponent, given in Eq. (50), versus the asymmetry parameter α.

$S \equiv S(\mu,\nu)$ satisfies the partial differential equation

$$\partial_\mu \partial_\nu S = S + \alpha(\partial_\mu S - \partial_\nu S)\,. \tag{39}$$

We now repeat the steps leading to (13) and find that the double Laplace transform, defined in (12), is given by

$$\widehat{S}(p,q) = \frac{1+\alpha(p^{-1}-q^{-1})}{pq+\alpha(q-p)-1}\,. \tag{40}$$

Since the governing equation (39) is no longer symmetric in the variables μ and ν, the Laplace transform (40) is not symmetric when $\alpha \neq 0$. We thus reiterate that results are quoted only for squares.

To invert the Laplace transform (40), we split the numerator $1+\alpha(p^{-1}-q^{-1})$ into $q-$dependent and $p-$dependent terms: $1-\alpha\, q^{-1}$ and $\alpha\, p^{-1}$. Due to asymmetry, these two are no longer equivalent, and the average number of sticks in the jammed state $S \equiv S(\nu,\nu)$ is given by

$$S = I + J\,. \tag{41}$$

The quantity $I \equiv I(\nu,\nu)$ is obtained by inverting $\big(1-\alpha\, q^{-1}\big)/[pq+\alpha(q-p)-1]$ first with respect to the conjugate variable p and then with respect to the conjugate variable q. Similarly, the quantity $J \equiv J(\nu,\nu)$ is obtained by inverting $\alpha\, p^{-1}/[pq+\alpha(q-p)-1]$ first with respect to q and then, with respect to p.

To compute the first term in (41), we follow the calculations in the symmetric case, and find that I is an integral of the form (15), specified by $F(q) = q^{-1}$ and

$$f(q) = q - \alpha + \frac{\beta^2}{q-\alpha}\,, \qquad \beta = \sqrt{1-\alpha^2}\,. \tag{42}$$

The saddle point is simply $q_* = \beta + \alpha$, and from the general formula (17) we obtain

$$I \simeq \frac{\beta}{\beta+\alpha}\,\frac{e^{2\beta\nu}}{\sqrt{4\pi\beta\nu}}\,. \tag{43}$$

This asymptotic behavior resembles (1) in that the leading exponential behavior is suppressed by a logarithmic term.

The second quantity in (41) is analogous in form to (15): it is given by an integral over p, rather than q,

$$J = \int_{-\mathrm{i}\infty}^{\mathrm{i}\infty} \frac{dp}{2\pi\mathrm{i}}\, G(p)\, e^{\nu g(p)}\,, \tag{44}$$

with the functions

$$G(p) = \frac{\alpha}{p(p+\alpha)}, \qquad g(p) = p + \alpha + \frac{\beta^2}{p+\alpha}\,. \tag{45}$$

However, the saddle point of the function $g(p)$ is different, $p_* = \beta - \alpha$. To evaluate the integral J, we simply replace $F(q_*)$, $f(q_*)$, and $f''(q_*)$ in (17) with $G(p_*)$, $g(p_*)$, and $g''(p_*)$ respectively, to find

$$J \simeq \frac{\alpha}{\beta-\alpha}\,\frac{e^{2\beta\nu}}{\sqrt{4\pi\beta\nu}}\,. \tag{46}$$

Therefore, the two terms in the sum (41) are proportional to each other, and by adding (43) and (46), we arrive at

$$S \simeq C\,\frac{e^{2\beta\nu}}{\sqrt{4\pi\beta\nu}}\,, \qquad C = \frac{1}{2(\alpha_c^2-\alpha^2)}\,, \tag{47}$$

with the critical point α_c given in (37). The constant C diverges as $\alpha \uparrow \alpha_c$, thereby indicating that the result (47) is valid only when the asymmetry is sufficiently weak, $\alpha < \alpha_c$. Indeed, the integrand in (44) has two simple poles: one at $p = -\alpha$ and another at $p = 0$. The first pole is located to the left of the saddle point p_*, irrespective of α. However, the second pole is located to the left of the saddle point only when $\alpha < \alpha_c$, and consequently, Eq. (46) holds only in this regime.

To evaluate the integral J when $\alpha > \alpha_c$, we deform the integration contour so that it consists of a line parallel to the imaginary axis which passes through the saddle point p_* and a small circle enclosing the origin, $p = 0$. The residue at the origin gives the dominant contribution, $J \simeq e^{\nu/\alpha}$, which is valid when the asymmetry is

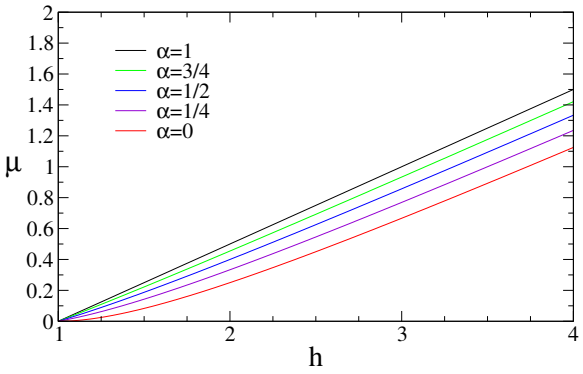

FIG. 10: The scaling exponent, given in Eq. (52), versus the moment index h for various values of the asymmetry parameter α.

sufficiently strong, $\alpha > \alpha_c$. In this regime, the quantity I in (43) is negligible, and consequently, $S(\nu,\nu) \simeq e^{\nu/\alpha}$.

In summary, the number of sticks in the jammed state state grows algebraically with area A

$$S \simeq U\, A^{\gamma}, \quad \text{with} \quad \gamma = \begin{cases} \sqrt{1-\alpha^2} & \alpha \le \alpha_c\,, \\ 1/(2\alpha) & \alpha \ge \alpha_c\,. \end{cases} \tag{48}$$

As long as there is some asymmetry, the growth is sublinear: $\gamma < 1$ when $\alpha > 0$. The exponent γ is continuous at the critical point, but its first derivative is discontinuous at that point. Furthermore, the exponent γ is concave when $\alpha < \alpha_c$ but it is convex when $\alpha > \alpha_c$. The critical value is $\gamma_c = \alpha_c$, and the convergence toward the leading asymptotic behavior is slower near the critical point (Fig. 8).

The prefactor U in (48) depends logarithmically on area in the weakly asymmetric phase, but it is independent of the area in the strongly asymmetric case. This prefactor is given by

$$U = \begin{cases} C/\sqrt{2\pi\beta \ln A} & \alpha < \alpha_c, \\ U_c & \alpha = \alpha_c, \\ 1 & \alpha > \alpha_c\,. \end{cases} \tag{49}$$

The constant C is quoted in (47). Hence, there is logarithmic correction in the weakly asymmetric phase, but the logarithmic correction disappears in the strongly asymmetric phase. Numerically, we estimate the critical prefactor $U_c \approx 0.4$ and we note the "double discontinuity": the critical value U_c does not match either of the limiting behaviors. On the one hand, we have $U \to 0$ as $\alpha \uparrow \alpha_c$ in the large-area limit $A \to \infty$, and on the other hand, we have $U \to 1$ as $\alpha \downarrow \alpha_c$.

The length distribution decays algebraically

$$P_k \simeq V\, k^{-\sigma}, \quad \text{with} \quad \sigma = 1 + \beta - \alpha\,, \tag{50}$$

for $k \gg 1$. This behavior is derived in Appendix B. The power-law tail (50) generally holds for infinitely large systems. However, for finite systems, this behavior holds

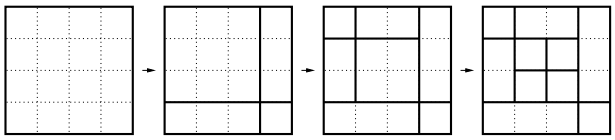

FIG. 11: Illustration of the fragmentation process (53). Initially, the system consists of a single rectangle. Through a series of random fragmentation events, the system arrives at a jammed state where all rectangles are sticks with minimal horizontal or vertical size.

in the range $\ln k \ll \sqrt{\ln n}$, as discussed above. Generally, the exponent σ decreases monotonically as α increases, and it vanishes in the completely asymmetric case (Fig. 9). Therefore, as the asymmetry parameter becomes smaller, the tail of the length distribution decays more sharply (see also Ref. [26]).

Interestingly, the exponent σ which characterizes the tail of the length distribution has the same form (50) in the weakly asymmetric phase, $\alpha \le \alpha_c$ and the strongly asymmetric phase $\alpha \ge \alpha_c$. Yet, the prefactor V in (50) depends algebraically on area in the strongly asymmetric phase, but it is independent of the area in the weakly asymmetric phase. This prefactor is given by

$$V = \begin{cases} 2\beta(\alpha_c^2 - \alpha^2) & \alpha < \alpha_c\,, \\ \sqrt{\beta/(2\pi U_c^2 \ln A)} & \alpha = \alpha_c \\ \sqrt{\beta/(2\pi \ln A)}\, A^{\beta - 1/(2\alpha)} & \alpha > \alpha_c\,. \end{cases} \tag{51}$$

Therefore, the length distribution depends on system size in the strongly asymmetric phase, but it is independent of system size in the weakly asymmetric phase.

From the length distribution P_k, it is also possible to evaluate the moments M_h defined in (31). We find that the moments grow algebraically with the area as in (34), $M_h \sim A^{\mu}$. For asymmetric fragmentation, the spectrum of scaling exponents is given by

$$\mu = \frac{\beta^2}{2(h+\alpha)} + \frac{h+\alpha}{2} - 1\,. \tag{52}$$

This spectrum reduces to (34) when fragmentation is symmetric, but in contrast, the scaling exponents are linear, $\mu = \frac{h-1}{2}$, when fragmentation is completely asymmetric. Figure 10 demonstrates how multi-scaling becomes less pronounced as the asymmetric nature of the fragmentation process becomes stronger.

IV. FRAGMENTATION INTO FOUR RECTANGLES

The fragmentation process (2) incorporates two stochastic elements as both the fragmentation point and the fragmentation direction are selected at random. The latter element can be eliminated by generating four rectangles, rather than two, in each fragmentation event

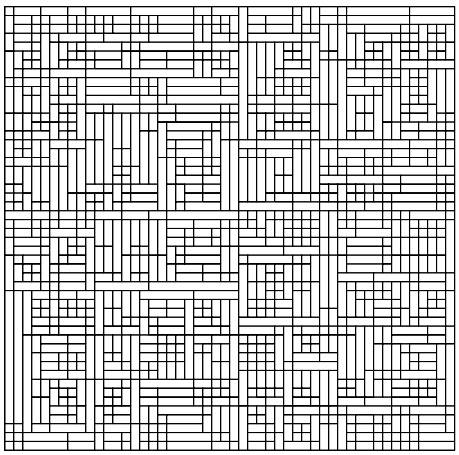

FIG. 12: A jammed configuration in a system of size 50×50.

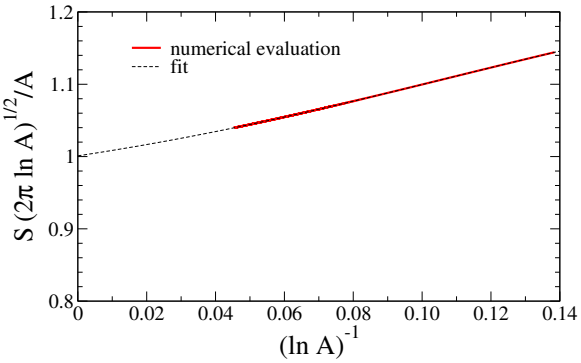

FIG. 13: The quantity $S\sqrt{2\pi \ln A}/A$ versus $(\ln A)^{-1}$. The dashed line shows results of a fourth-order polynomial fit to the data. Results of numerical evaluation of the recursion equation (54) agrees with the theoretical prediction for the leading asymptotic behavior to within 0.1%.

(Fig. 11). A continuous version of this planar fragmentation process and related variants were analyzed in a number of studies [29–34].

We now address this natural counterpart of the fragmentation process (2) where first an internal grid point is selected at random, and then, two simultaneous cuts are made, one in the horizontal direction and one in the vertical direction. As a result, each fragmentation event generates four rectangles (Fig. 11)

$$(m,n) \to (i,j)+(m-i,j)+(i,n-j)+(m-i,n-j)\,, \quad (53)$$

with randomly selected $1 \le i \le n-1$ and $1 \le j \le m-1$. In contrast with (2), once the grid point is selected, the outcome is deterministic. Again, rectangles with $m > 1$ and $n > 1$ are active and otherwise, rectangles with $m = 1$ or $n = 1$ are frozen. Starting with a single $m \times n$ rectangle, the system eventually reaches a jammed state where all rectangles are sticks, including minimal 1×1 rectangles (Fig. 12).

The average number of frozen sticks in the jammed state, $S(m,n)$, satisfies the recursion equation

$$S(m,n) = \frac{4}{(m-1)(n-1)} \sum_{i=1}^{m-1} \sum_{j=1}^{n-1} S(i,j)\,, \qquad (54)$$

subject to the boundary conditions (4). For small rectangles, the recursion equation gives $S(2,2) = 4$, $S(3,3) = 7$, $S(4,4) = \frac{32}{3}$, and so on. In contrast with the fragmentation process (2) where the average number of sticks for narrow but long rectangles diverges logarithmically, these quantities are now finite, and for example, $S(2,n) = 4$ and $S(3,n) = 10 - \frac{6}{n-1}$. In general, we find the limiting values

$$\lim_{n\to\infty} S(m,n) = \frac{m(m+1)(m+2)}{6}\,, \qquad (55)$$

from the recursion equation (54).

For large rectangles, the recursion equation (54) turns into the partial differential equation

$$\partial_m \partial_n [mnS(m,n)] = 4S(m,n)\,. \qquad (56)$$

Using the logarithmic variables (10), we transform this equation into a partial differential equation with constant coefficients, $\partial_\mu \partial_\nu S + \partial_\mu S + \partial_\nu S = 3S$. By repeating the steps leading to (13), we obtain the Laplace transform

$$\widehat{S}(p,q) = \frac{1}{pq}\,\frac{(p+1)(q+1)-1}{(p+1)(q+1)-4}\,. \qquad (57)$$

Next, we rewrite this expression as a sum of two terms: $(2^{-1}+q^{-1})/(pq+p+q+3)$ and $(2^{-1}+p^{-1})/(pq+p+q+3)$. For squares, these two terms are equivalent and it suffices to perform the inverse Laplace transform of the first term with respect to p and then, with respect to q. We thus obtain $S(\nu,\nu) = I$ where I is given by the general integral (17). The integrand is specified by the functions

$$F(q) = \frac{q+2}{q(q+1)} \quad \text{and} \quad f(q) = q - 1 + \frac{4}{q+1}\,. \qquad (58)$$

From the condition $f'(q_*) = 0$ we notice that the saddle point remains $q_* = 1$, and by using (17), we find the leading asymptotic behavior of the number of frozen sticks in the jammed state (Fig. 13)

$$S \simeq \frac{3A}{\sqrt{4\pi \ln A}}\,. \qquad (59)$$

In comparison with (1), the average number of frozen sticks is now $3/\sqrt{2} \approx 2.12132$ times larger. Results of numerical evaluation of the recursion equation (54) are in excellent agreement with the theoretical prediction (59). As was the case for stochastic fragmentation, the average number of jammed rectangles (59) extends to all rectangles with a finite aspect ratio in the large-area limit.

For completeness, we quote the exact distribution of stick length

$$P_k = \frac{4}{3k(k+1)}\,, \qquad (60)$$

for $k > 1$ and $P_1 = \frac{1}{3}$. This form, which is realized in the limit $n \to \infty$, can be obtained using the method outlined in Appendix A. Sticks with $k \geq 2$ are doubly degenerate compared with minimal 1×1 rectangles and hence, the quantity P_1 is suppressed by a factor 2. The length distribution has a power-law tail, $P_k \simeq \frac{4}{3}k^{-2}$, which can be established using continuum analysis used to obtain (29). For a finite system, the power-law tail holds when $1 \ll k \ll \sqrt{\ln n}$, while at larger length scales the distribution is strongly suppressed by a log-normal term.

The planar fragmentation processes considered in this investigation generate special tilings of two-dimensional domains. Indeed, in the jammed configuration, sticks of unit width and variable length cover the original rectangle (Figures 2 & 12). The jammed configurations differ from those in the heavily studied dimer tiling [35–41] in two respects. First, the lengths of the sticks do vary dramatically [42–45]. Second, whereas in equilibrium problems jammed configurations are given equal weights, fragmentation is a dynamical process, and the different tiling configurations are generally realized with different probabilities.

The central quantity in tiling problem is the total number of jammed configurations which typically grows exponentially with area. For the process (53), it is straightforward to show that $T(m,n)$, the total number of jammed configurations for a rectangle of size $m \times n$, satisfies the recursion equation

$$T(m,n) = \sum_{\substack{1\leq i\leq m-1\\ 1\leq j\leq n-1}} T(i,j)T(m-i,j)T(i,n-j)T(m-i,n-j). \tag{61}$$

This recursion applies for all $m \geq 2$ and $n \geq 2$, and it is subject to the boundary conditions $T(m,1) = 1$ for all $m \geq 1$ and $T(1,n) = 1$ for all $n \geq 1$. As illustrated in Fig. 14, for any jammed configuration, the first fragmentation event can be uniquely identified. This first fragmentation event divides the original rectangle to four smaller and independent rectangles, thereby leading to the recursion (61). The same does not hold true for the fragmentation process (2) and for this reason, it is not possible to write closed recursion equations for the corresponding of number of jammed states.

A single iteration of the recursion (61) yields the number of jammed configurations for ladders, $T(2,n) = n - 1$, and a second iteration yields $T(3,n) = \frac{1}{3}(n-2)(n^2-4n+15)$. The exact expression

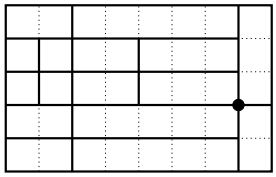

FIG. 14: Illustration of the fragmentation process (53). The first fragmentation event can always be uniquely identified.

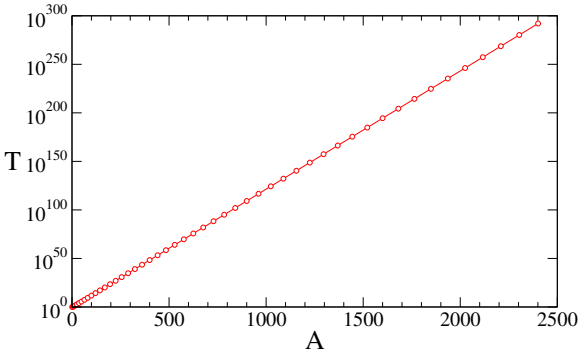

FIG. 15: The total number of jammed configurations for squares, $T = T(n,n)$, obtained by numerical iteration of (61), versus the area $A = n^2$.

n	1	2	3	4	5	6	7	8
$T(n,n)$	1	1	4	33	436	9,524	354,224	23,097,969

TABLE I: The number of jammed states for small squares.

for $T(4,n)$ is a seventh-order polynomial, and $T(m,n)$ quickly become unwieldy when m increases.

Table I lists the number of jammed configurations for squares with $n \leq 7$. Numerical iteration of the recursion (61) shows that the number of jammed configurations grows exponentially with area (see Fig. 15)

$$T \sim e^{\lambda A}. \tag{62}$$

For squares, the value $\lambda = 0.2805$ is obtained by fitting the numerically evaluated quantity $T(n,n)$ to an exponential.

V. DISCUSSION

In summary, we studied planar fragmentation, which can be viewed as dual to planar aggregation [46]. We obtained analytically several properties of the jammed state including the average number of rectangles, and the length distribution of rectangles. In general, statistical properties become independent of the aspect ratio in the large-area limit. Moreover, the length distribution of rectangles in the jammed state has a power-law tail, and the moments of this distribution exhibit multiscaling.

We also found a phase transition when the fragmentation process is asymmetric. Generally, the average number of jammed rectangles grows sub-linearly with system size, and the exponent characterizing this growth varies continuously with the asymmetry parameter. This exponent is concave in the weakly asymmetric phase and convex in the strongly asymmetric phase. In addition, The length distribution is independent of system size in the weakly asymmetric phase, but it does depend on system size in the strongly asymmetric phase.

Our theoretical analysis relies on recursion equations that describe the final state of the system. Since each

fragmentation event involves a single rectangle, the recursion equations are linear. For large systems, we employed the continuum approach and then applied the Laplace transform to obtain exact results for the leading asymptotic behavior. Numerical evaluation of the recursion equations support the theoretical predictions.

The recursion equations bypass the evolution toward the jammed state and hence, directly yield statistics of the final configuration. The fragmentation rate may be an arbitrary function of the area, yet, as long as the fragmentation point is selected at random, the recursion equation (3) holds. For specific fragmentation rates, it is natural to study the evolution towards the jammed state, including in particular the average jamming time, and the distribution of jamming times.

Our analysis yields statistics of *single* fragments in the jammed state such as the first moment and the length distribution. Missing from our analysis, however, are statistics of *multiple* fragments such as correlations between the orientations of neighboring sticks. Both sets of statistics are relevant for characterizing the geometrical structure of planar fragmentation patterns found in martensitic transformations [26], breakage of brittle objects [47, 48], cracking of soils [49], and drying of suspensions [50].

The behavior in higher dimensions can be studied as well. In the three-dimensional generalization of (2), the jammed state consists of rectangular plates, that is, boxes with unit width. In this case, we find that the average number F of frozen boxes grows as

$$F \simeq \left(\frac{\sqrt{3}}{2}\right)^3 \frac{V}{\pi \ln V}\,, \tag{63}$$

with V the volume of the original box. The area distribution of jammed plates represents an interesting challenge.

The process (53) can be also generalized to d dimensions. Here, each fragmentation event generates 2^d boxes. The jammed state consists of frozen boxes, each of which has at least one minimal side. The number of frozen boxes F grows as

$$F \simeq \frac{2^d-1}{\sqrt{d}}\,\frac{V}{\left(\frac{4\pi}{d}\,\ln V\right)^{(d-1)/2}}\,. \tag{64}$$

This result, which generalizes (59), is derived in Appendix C. A frozen box is characterized by $d-1$ nontrivial lengths and it is an interesting challenge to characterize the distribution of these lengths.

We thank Jean-Marc Luck for helpful comments. This work was supported in part by the US Department of Energy through the Los Alamos National Laboratory. Los Alamos National Laboratory is operated by Triad National Security, LLC, for the National Nuclear Security Administration of U.S. Department of Energy (Contract No. 89233218CNA000001).

[1] F. Brauer, C. P. Dullemond, and T. Henning, Astronomy and Astrophys. **480**, 859 (2008).
[2] N. Brilliantov, P. L. Krapivsky, A. Bodrova, F. Spahn, H. Hayakawa, V. Stadnichuk, and J. Schmidt, Proc. Natl. Acad. Sci. **112**, 9536 (2015).
[3] J. M. Zheng, M. Gu, J. Xiao, P. J. Zuo, C. M. Wang, and Z. G. Zhang, Nano Lett. **13**, 3824 (2013).
[4] J. Krauss, R. Bommarco, M. Guardiola et al, Ecology Lett. **13**, 597 (2010).
[5] L. Fehrig, Ann. Rev. Ecol. Evol. Systm. **48**, 1 (2017).
[6] K. Kawagoe, G. Huber, M. Pradas, M. Wilkinson, A. Pumir, and E. Ben-Naim, Phys. Rev. E **96**, 012142 (2017).
[7] F. Taubert, F. Fischer, J. Groeneveld, et al, Nature **554**, 519 (2018).
[8] G. Moad, E. Rizzardo, and S. H. Thang, Polymer **49**, 1079 (2008).
[9] P. W. Miller and N. T. Ouelette, Phys. Rev. E **89**, 042806 (2014).
[10] F. Ginot, I. Theurkauff, I. Detcheverry, C. Ybert, and C. Cottin-Bizonne, Nature Comm. **9**, 696 (2018).
[11] R. C. Hidalgo and I. Pagonabarraga, Phys. Rev. E **77**, 061305 (2008).
[12] F. Spahn, N. Albers, M. Sremcevic, and C. Thornton, Europhys. Lett. **67**, 545 (2004).
[13] H. J. Herrmann and F. Kun, Phys. Rev. E **59**, 2623 (1999).
[14] J. A. Astrom, R. P. Linna, J. Timonen, P. F. Moller, and L. Oddershede, Phys. Rev. E **70**, 026104 (2004).
[15] J. R. Gladden, N. Z. Handzy, A. Belmonte, and E. Vllermaux, Phys. Rev. Lett. **94**, 035503 (2005).
[16] A. F. Filippov, Theory Prob. Appl. **6**, 275 (1961).
[17] E. D. Mcgrady and R. M. Ziff, J. Phys. A **18**, 3027 (1985).
[18] Z. Cheng and S. Redner, Phys. Rev. Lett. **60**, 2450 (1988).
[19] P. L. Krapivsky, S. Redner and E. Ben-Naim, *A Kinetic View of Statistical Physics* (Cambridge: Cambridge University Press, 2010).
[20] K. M. Crosby and R. M. Bradley, Phys. Rev. E **55**, 6084 (1997).
[21] Zhao Qin, N. M. Pugno, and M. J. Buehler, Sci. Rep. **4**, 4966 (2015).
[22] J. M. Ball, P. Cesana, and B. Hambly, MATEC Web Conferences **33**, 02008 (2015).
[23] P. Cesana and B. Hambly, arXiv:1810.04380.
[24] M. Rao, S. Sengupta, and H. K. Sahu, Phys. Rev. Lett. **75**, 2164 (1995).
[25] E. Ben-Naim and P. L. Krapivsky, Phys. Rev. Lett. **76**, 3234 (1996).
[26] G. Torrents, X. Illa, E. Vives, and A. Planes, Phys. Rev. E **95**, 013001 (2017).
[27] E. Limpert, W. A. Stanel, and M. Abbt, BioSci. **51**, 341 (2001)
[28] M. Mitzenmacher, Internet Math. **1**, 226 (2003).
[29] G. Tarjus and P. Viot, Phys. Rev. Lett. **67**, 1875 (1991).
[30] P. L. Krapivsky and E. Ben-Naim, Phys. Rev. E **50**, 3502

(1994).
[31] G. J. Rodgers and M. K. Hassan, Phys. Rev. E **50**, 3459 (1994).
[32] D. Boyer, G. Tarjus, and P. Viot, Phys. Rev. E **51**, 1043 (1995).
[33] D. Boyer, G. Tarjus, and P. Viot, J. Physique **7**, 13 (1997).
[34] E. Ben-Naim and P. L. Krapivsky, Physica D **107**, 156 (1997).
[35] P. W. Kasteleyn, Physica **27**, 1209 (1961).
[36] M. E. Fisher and H. Temperley, Phil. Mag. **6**, 1061 (1961).
[37] M. E. Fisher and J. Stephenson, Phys. Rev. **132**, 1411 (1963).
[38] E. H. Lieb, J. Math. Phys. **8**, 2339 (1967).
[39] R. J. Baxter, J. Math. Phys. **9**, 650 (1968).
[40] H. Cohn, N. Elkies, and K. Propp, Duke Math. J. **85**, 117 (1996).
[41] H. Cohn, R. Kenyon, and K. Propp, J. Amer. Math. Soc. **14**, 297 (2001).
[42] O. J. Heilmann and E. H. Lieb, Commun. Math. Phys. **25**, 190 (1972).
[43] M. Jerrum, J. Stat. Phys. **48**, 1 (1987).
[44] F. Y. Wu, Phys. Rev. E **74**, 020104 (2006).
[45] A. Giuliani, I. Jauslin, and E. H. Lieb, J. Stat. Phys. **163**, 211 (2016).
[46] D. S. Ben-Naim, E. Ben-Naim, and P. L. Krapivsky, J. Phys. A **51**, 455002 (2018).
[47] N. Vanderberghe and E. Villermaux, Soft Matter **34**, 8162 (2013).
[48] L. Dias and F. Parisio, Phys. Rev. E **90**, 032405 (2014).
[49] S. Bohn, L. Pauchard, and Y. Couder, Phys. Rev. E **71**, 046214 (2005).
[50] A. Nakahara and Y. Matsuo, Phys. Rev. E **74**, 045102(R) (2006).

Appendix A: Length Distribution

To obtain the length distribution for an infinite system, we treat m and n as discrete variables. To this end, we introduce the generating function

$$\mathcal{S}(x,y) = \sum_{m\geq 1}\sum_{n\geq 1} S(m,n)\, x^{m-1}y^{n-1}\,. \qquad \text{(A1)}$$

The generating function $\mathcal{S} \equiv \mathcal{S}(x,y)$ satisfies the partial differential equation

$$\partial_x\partial_y\mathcal{S} = (1-x)^{-1}\,\partial_y\mathcal{S} + (1-y)^{-1}\,\partial_x\mathcal{S}\,. \qquad \text{(A2)}$$

To obtain this equation, we multiply the recursion equation (3), that governs the averages $S(m,n)$, by $(m-1)(n-1)x^{m-2}y^{n-2}$ and sum over $m\geq 2$ and $n\geq 2$. Furthermore, equation (A2) is subject to the boundary conditions $\mathcal{S}(x,0) = x/(1-x)$ and $\mathcal{S}(0,y) = y/(1-y)$.

We now introduce the variables

$$\xi = -\ln(1-x), \quad \eta = -\ln(1-y)\,. \qquad \text{(A3)}$$

This transformation turns (A2) into a partial differential equation with constant coefficients

$$\partial_\xi\partial_\eta\mathcal{S} = \partial_\xi\mathcal{S} + \partial_\eta\mathcal{S}\,, \qquad \text{(A4)}$$

while the boundary conditions become $\mathcal{S}(\xi,0) = e^\xi - 1$ and $\mathcal{S}(0,\eta) = e^\eta - 1$. Next, we introduce the double Laplace transform

$$\widehat{\mathcal{S}}(p,q) \;=\; \int_0^\infty d\xi\, e^{-p\xi}\int_0^\infty d\eta\, e^{-q\eta}\,\mathcal{S}(\xi,\eta)\,. \qquad \text{(A5)}$$

Using the governing equation (A4), we obtain

$$\widehat{S}(p,q) = \frac{p^{-1}+q^{-1}}{pq-p-q}. \qquad \text{(A6)}$$

We now invert the Laplace transform with respect to one of the conjugate variables, to obtain the sum

$$\begin{aligned}\mathcal{S}(\xi,\eta) \;&=\; \int_{-\mathrm{i}\infty}^{\mathrm{i}\infty}\frac{dq}{2\pi\mathrm{i}}\,\frac{1}{q(q-1)}\,e^{\eta q+\xi q/(q-1)}\\ &+\; \int_{-\mathrm{i}\infty}^{\mathrm{i}\infty}\frac{dp}{2\pi\mathrm{i}}\,\frac{1}{p(p-1)}\,e^{\xi p+\eta p/(p-1)}\,.\end{aligned}$$

Thus far, our analysis is exact and in particular, it applies to all m and n. We now restrict our attention to squares, $\xi = \eta$ and further, we focus on the leading asymptotic behavior for large systems which is captured by the leading behavior when $\eta\to\infty$. By performing the inverse Laplace transform over the second conjugate variable, we obtain

$$S(\eta,\eta) \simeq \frac{e^{4\eta}}{\sqrt{4\pi\eta}}. \qquad \text{(A7)}$$

Next, we analyze the length distribution $S_k(m,n)$. Its corresponding generating function satisfies Eq.(A4), subject to the boundary conditions $\mathcal{S}_k(\xi,0) = (1-e^{-\xi})^{k-1}$ $S_k(0,\eta) = (1-e^{-\eta})^{k-1}$. These two boundary conditions follow from $\mathcal{S}_k(x,0) = x^{k-1}$ and $\mathcal{S}_k(0,y) = y^{k-1}$. By repeating the steps leading to (A6), we obtain

$$\widehat{\mathcal{S}}_k(p,q) = \frac{\Gamma(k)}{pq-p-q}\left[\frac{(q-1)\Gamma(q)}{\Gamma(k+q)} + \frac{(p-1)\Gamma(p)}{\Gamma(k+p)}\right].$$

We can verify that $\mathcal{S}(p,q) = \sum_{k\geq 2}\mathcal{S}_k(p,q)$, whereas the corresponding quantity in (24), which is obtained by treating the variables m and n as continuous, violates this normalization. The leading asymptotic behavior in the limit $\eta\to\infty$ is given by

$$\mathcal{S}_k(\eta,\eta) \simeq \frac{2}{k(k+1)}\,\frac{e^{4\eta}}{\sqrt{4\pi\eta}}\,. \qquad \text{(A8)}$$

The average number of sticks does not depend on aspect ratio and thus, we assume $S_k(m,n) \simeq P_k S(m,n)$ at large sizes. Then, according to the definition (A1) and the leading asymptotic behavior (A7) we have $\mathcal{S}_k(\eta,\eta) \simeq P_k e^{4\eta}/\sqrt{4\pi\eta}$. By comparing this expression with (A8), we deduce the length distribution P_k in (30).

Appendix B: Asymmetric fragmentation

The average number of sticks with a given length satisfies the partial differential equation (3) subject to the boundary conditions (23). The double Laplace transform, defined by (12), is given by

$$\widehat{S}_k(p,q) = \frac{(q-\alpha)k^{-1-q} + (p+\alpha)k^{-1-p}}{pq + \alpha(q-p) - 1}\,. \qquad \text{(B1)}$$

To perform the double inverse Laplace transform, we rewrite the numerator as a sum of the q-dependent quantity $(q-\alpha)k^{-1-q}$ and the p-dependent quantity $(p+\alpha)k^{-1-p}$. The quantity $S_k(p,q)$ is therefore a sum of two terms as in (41).

The first term in the sum (41) is the integral I defined in (15) with $F(q)=1$ and

$$f(q) = q - \alpha + \frac{\beta^2}{q-\alpha} - (1+q)x\,. \qquad \text{(B2)}$$

Here, we again used the notations $\beta = \sqrt{1-\alpha^2}$ and $x = \ln k/\ln n$. The saddle point of the function $f(q)$ is $q_* = \beta(1-x)^{-1/2} + \alpha$ and with (17), we arrive at

$$\begin{aligned} I &= \frac{\exp\left[\nu\left(2\beta\sqrt{1-x} - x - \alpha x\right)\right]}{\sqrt{4\pi\nu(1-x)^{3/2}/\beta}} \\ &\simeq \frac{\sqrt{\beta}}{\sqrt{4\pi\nu}}\, e^{2\beta\nu}\, k^{-(1+\beta+\alpha)}\,. \end{aligned} \qquad \text{(B3)}$$

By evaluating the small-x behavior of the general expression in the first line, we obtained the large-k behavior in the second line.

The second term in the sum (41) is the integral J defined in (44) with $G(p)=1$ and

$$g(p) = p + \alpha + \frac{\beta^2}{p+\alpha} - (1+p)x\,. \qquad \text{(B4)}$$

The saddle point of the function $g(p)$ is $p_* = \beta(1-x)^{-1/2} - \alpha$. By using the analog of the general expression (17), we obtain

$$\begin{aligned} J &= \frac{\exp\left[\nu\left(2\beta\sqrt{1-x} - x + \alpha x\right)\right]}{\sqrt{4\pi\nu(1-x)^{3/2}/\beta}} \\ &\simeq \sqrt{\frac{\beta}{4\pi\nu}}\, e^{2\beta\nu}\, k^{-(1+\beta-\alpha)}\,. \end{aligned} \qquad \text{(B5)}$$

The large-k behavior in the second line follows from the small-x behavior in the first line. By comparing the tails (B3) and (B5), we conclude that I is negligible compared with J, and therefore $S_k(\nu,\nu) \simeq J$ for sufficiently large k. The power-law tail (50) follows from $P_k = S_k(\nu,\nu)/S(\nu,\nu)$.

So far, we have not differentiated between horizontal sticks and vertical ones. When the fragmentation process is asymmetric as in (36), we expect more horizontal sticks than vertical ones when $\alpha > 0$, and that the opposite is true when $\alpha < 0$ (see Ref. [26]). The average number of horizontal sticks satisfies (39) with the boundary conditions $S_k(\mu,0) = e^{-\mu}\delta(\mu - \ln k)$ and $S_k(0,\nu) = 0$; similarly, the average number of vertical sticks satisfies (39) with the boundary conditions $S_k(\mu,0) = 0$ and $S_k(0,\nu) = e^{-\nu}\delta(\nu - \ln k)$. Let P_k^+ be the length-distribution of sticks of the dominant orientation and P_k^- be the length-distribution of sticks of the subdominant orientation. It is straightforward to show that the first term in the numerator of (B1) corresponds to the subdominant distribution, and that the second term in (B1) yields the dominant distribution. Thus, we have

$$P_k^+ \sim k^{-\sigma_-} \quad \text{and} \quad P_k^- \sim k^{-\sigma_+}. \qquad \text{(B6)}$$

with $\sigma_\pm = 1 + \beta \pm |\alpha|$. This tail behavior is compatible with equation (50) as $\sigma = \sigma_-$.

Appendix C: Arbitrary Dimensions

The process (53) can be generalized to d dimensions where in each fragmentation event a box breaks into 2^d boxes. This elementary event is repeated until a jammed state is reached. The recursion equation for the number of frozen boxes is a straightforward generalization of Eq. (54) and it includes d sums.

The multivariate Laplace Transform is given by a straightforward generalization of (57)

$$\widehat{S}(q_1, q_2, \ldots, q_d) = \frac{\prod_{\ell=1}^d (q_\ell + 1) - 1}{\prod_{\ell=1}^d (q_\ell + 1) - 2^d} \times \prod_{\ell=1}^d \frac{1}{q_\ell}\,. \qquad \text{(C1)}$$

The inverse Laplace transform is a $d-$fold integral, and we first invert this multivariate transform with respect to the conjugate variable q_d. Further, we restrict our attention hyper-cubes for which $\ln n_\ell = \nu$ for all ℓ, and then

$$S = \int_{-\mathrm{i}\infty}^{\mathrm{i}\infty} \frac{dq_1}{2\pi\mathrm{i}} \cdots \int_{-\mathrm{i}\infty}^{\mathrm{i}\infty} \frac{dq_{d-1}}{2\pi\mathrm{i}}\, \Phi(\mathbf{q})\, e^{\nu\phi(\mathbf{q})}\,. \qquad \text{(C2)}$$

Here, we introduced the shorthand notation $\mathbf{q} = (q_1, \ldots, q_{d-1})$ and

$$\phi(\mathbf{q}) = \sum_{\ell=1}^{d-1} q_\ell - 1 + \frac{2^d}{\prod_{\ell=1}^{d-1}(q_\ell+1)}\,. \qquad \text{(C3)}$$

The saddle point is $\mathbf{q}_* = (1, \ldots, 1)$, and at this point, it is easy to show that $\phi(\mathbf{q}_*) = d$ and $\Phi(\mathbf{q}_*) = (2^d - 1)/2^{d-1}$. We tacitly do not display the function $\Phi(\mathbf{q})$ because only its value at the saddle point is needed.

To evaluate the integral (C2), we expand $\phi(\mathbf{q})$ near the saddle point using $q_\ell = 1 + \mathrm{i}u_\ell/\sqrt{\nu}$, and then,

$$\phi(\mathbf{u}) \simeq d - \frac{U(\mathbf{u})}{\nu}, \quad U(\mathbf{u}) = \frac{1}{2}\sum_{a=1}^{d-1}\sum_{b=1}^{a} u_a u_b\,. \qquad \text{(C4)}$$

The Gaussian integral can be computed in arbitrary dimension,

$$\int_{-\infty}^{\infty} du_1 \cdots \int_{-\infty}^{\infty} du_{d-1} e^{-U(\mathbf{u})} = \frac{(4\pi)^{(d-1)/2}}{\sqrt{d}}. \qquad \text{(C5)}$$

The computation of the Gaussian integral relies on the fact that the $(d-1)\times(d-1)$ matrix associated with the quadratic form $U(\mathbf{u})$ has eigenvalues $\frac{1}{2}(d,1,\ldots,1)$. The integral (C5) completes the derivation of (64).